Lattice Dynamics of Mg_2Pb at Room Temperature*

N. Wakabayashi and A. A. Z. Ahmad†
Solid State Division, Oak Ridge National Laboratory, Oak Ridge, Tennessee 37830

and

H. R. Shanks and G. C. Danielson
Institute for Atomic Research and Department of Physics, Iowa State University, Ames, Iowa 50010

(Received 7 October 1971)

The phonon-dispersion curves along the [001], [110], and [111] directions in Mg_2Pb at room temperature have been measured by neutron inelastic scattering. Although these curves are qualitatively similar to those for Mg_2Sn, marked differences exist in some of the longitudinal branches which show large dips at small q for Mg_2Pb, suggesting large screening effects of free carriers. A reasonable fit to the measured dispersion curves has been obtained with a nine-parameter shell model. The model was used to calculate the phonon density of states and the temperature dependence of the Debye temperature. The calculated Debye temperature agreed well with the Debye temperature obtained from heat-capacity measurements.

I. INTRODUCTION

Mg_2Pb is an intermetallic compound belonging to the family Mg_2X with X being Si, Ge, Sn, or Pb. Mg_2Si, Mg_2Ge, and Mg_2Sn are semiconductors with energy gaps of about 0.8, 0.7, and 0.3 eV. Stringer and Higgins have shown[1] that Mg_2Pb is a metal. Because of its relatively high carrier concentration of 10^{20} carriers/cm^3 compared to Mg_2Si, Mg_2Ge, and Mg_2Sn, it might be expected that the effects of screening on the phonon-dispersion curves would be larger for Mg_2Pb than for the other members of the family. From the results of Landau-quantum-oscillation measurements, the Thomas-Fermi reciprocal screening length k_s is estimated to be of the order of 0.1 reciprocal-lattice units. The phonon-dispersion curves for wave vectors smaller than this value should, therefore, show the influence of the free carriers. One of the purposes of this research was to see if the screening effect could be detected in Mg_2Pb. Also, since the phonon-dispersion relation for Mg_2Sn has been measured[2] recently using neutron inelastic scattering, it is of considerable interest to measure the phonon-dispersion relation for Mg_2Pb and to compare the results with those for Mg_2Sn.

Mg_2Pb has the antifluorite crystal structure which consists of three interpenetrating fcc lattices with a Pb ion at the origin and Mg ions at $(\frac{1}{4}, \frac{1}{4}, \frac{1}{4})a$ and $(-\frac{1}{4}, -\frac{1}{4}, -\frac{1}{4})a$, where the lattice constant a is equal to 6.836 Å. Since there are three atoms per unit cell, the phonon-dispersion relation will, in general, have nine branches for any phonon wave vector. Along the symmetry directions $\langle 001 \rangle$ and $\langle 111 \rangle$, the transverse branches are degenerate. With the $(1\bar{1}0)$ plane in the scattering plane, six different frequencies are observed for wave vectors along [001], [110], and [111] directions. Group-theoretical discussions of the lattice dynamics of this structure have been given in a paper by Kearney *et al.*[3] and the notation therein will be used in this paper.

II. CRYSTAL PREPARATION

Single crystals of Mg_2Pb were grown by the Bridgman method using a 5% excess of Mg to ensure growth of the stoichiometric β phase.[4] The starting materials were Pb, obtained from Cominco with a stated purity of 99.9999% and distilled Mg, obtained from the Dow Chemical Company. The Mg was redistilled in a vacuum of 10^{-9} Torr. Mass spectrometer analysis of the resulting Mg for minor impurities indicated a total impurity level of 40 ppm atomic, of which half was oxygen. The resistivity ratio of the redistilled metal was approximately 2000.

An analysis of the Mg_2Pb for major constituents was carried out on five samples. This analysis indicated that the samples were, within experimental error, stoichiometric Mg_2Pb. Photographs of the crystals taken at a magnification of 500× showed no evidence of any second-phase material, as found by Stringer and Higgins.[5]

An electron-microprobe analysis was also performed on the material to determine homogeneity. Analysis of samples which were kept under acetone until insertion in the vacuum system showed that the samples were homogeneous within the statistical error. Samples which were allowed to react with the atmosphere for a short period of time showed inhomogeneities similar to those reported by Stringer and Higgins.[5]

Because of the rapid reaction of Mg_2Pb with the atmosphere, the crystals had to be kept covered

at all times. The crystal used in this study had a volume of about 2 cm^3 and was mounted on a quartz plate with a low-vapor-pressure resin. Care was taken to ensure that the [110] axis of the crystal was perpendicular to the plane of the quartz plate. A small quartz bell jar filled with dry helium and a small amount of desiccant was placed over the sample and sealed to the quartz plate with low-vapor-pressure resin.

III. MEASUREMENTS AND ANALYSIS

Measurements reported here were made with two triple-axis neutron spectrometers, one at the Oak Ridge Research Reactor (ORR), and the other at the High Flux Isotope Reactor (HFIR). The sample was mounted on a holder with the $(1\bar{1}0)$ plane horizontal and measurements were made for wave vectors along the [001], [110], and [111] directions in the constant-Q mode of operation. Most of the acoustic modes were obtained at the ORR with the incident neutron energy fixed at 45 meV. Measurements at the HFIR were performed with the scattered neutron energy held fixed at 14, 24, or 28 meV. Most of the results were obtained with Soller-slit collimators 0.6° full width at half-maximum both before and after the sample. Bragg reflections from the (0002) planes of Be crystals were used as monochromator and analyzer.

For wave vectors along [001] and [111], the modes are purely longitudinal or transverse and the transverse modes are doubly degenerate. Therefore, there are only six distinct values of frequencies in these directions. In the [110] direction, most of the modes are of mixed polarizations and there are nine distinct frequencies. However, with the present orientation of the crystal, three branches with the polarization vectors perpendicular to the $(1\bar{1}0)$ plane could not be observed. The results of Kearney *et al.*[2] were helpful in choosing reciprocal-lattice points for which experimental conditions would be favorable.

The results of the measurements are shown in Table I and are plotted in Fig. 1. Errors listed are mainly due to statistical uncertainty in the scattered neutron counts. Some of the frequencies of the high-frequency branches could not be obtained because of high background counts and, possibly, of low structure factors. The longitudinal optic branches connected to Γ_{15} show considerable dips at small wave vectors, unlike those of Mg_2Sn, and their frequencies approach those of the transverse optic branches at Γ. This result strongly suggests the existence of large screening effects at long wavelengths since the Γ_{15} modes would be triply degenerate if the screening is complete.

However, over-all features of the dispersion curves are remarkably similar to those of Mg_2Sn. In view of this similarity, the present data were fitted with a nine-parameter shell model used by Kearney *et al.* for Mg_2Sn. The model includes the nearest Pb-Mg and Pb-Pb interactions and those between the nearest nonequivalent Mg atoms in the axially symmetric form. Only the polarizability of the Pb ion is taken into account. Fitting was tried with a model which included the polarizability of the Mg ions, but the shell parameters of the Mg ions became unrealistic and the model was abandoned. The same difficulty was experienced by Kearney *et al.*[1] in the case of Mg_2Sn. The solid lines in Fig. 1 show the fit with the nine-parameter shell model, and the values of the parameters of the model are given in Table II together with those for Mg_2Sn. Although the larger force-constant parameters A_1 and B_1 have values similar to those of Mg_2Sn, other constants are somewhat different. These differences may be due to an inadequacy of the model since the model does not provide a completely satisfactory fit to the experimental data for either material. As expected, the model fails to reproduce the observed frequencies of small-q phonons which are strongly influenced by the free-carrier screening.

IV. DISCUSSION

The frequency ν_R of the triply degenerate $\vec{q} = 0$ Raman-active phonon, Γ'_{25}, as determined by Raman-scattering technique,[6] has a value of 6.42 ± 0.015 THz which is in good agreement with the value 6.40 THz obtained from the present experiment.

Anastassakis and Burstein[7] have recently reported the results of resonance-Raman-scattering measurements on the longitudinal Γ_{15} phonon. Since this phonon is Raman inactive, they concluded that the value of the frequency in their measurement, 5.67 THz, should correspond to that of a phonon at a finite wave vector which was estimated to be about 2% of the reciprocal-lattice vector. This is in slight disagreement with the value of 5.4 THz estimated from the present result, assuming that the Γ_{15} is triply degenerate, as it should be if the free-carrier screening effect is complete. This discrepancy may be due to the difference in the carrier concentrations of the two samples used.

Anastassakis and Perry[8] estimated the value of the transverse Γ_{15} phonon frequency to be 5.5 ± 0.15 THz. This value does not agree with the present result of 5.1 ± 0.1 THz and, therefore, the model they used to estimate the frequency may be inadequate.

The elastic constants were calculated from the nine-parameter shell model and the results are compared with those determined by the ultrasonic technique (Table III).[9] The uncertainties in the calculated values are large since the phonon frequencies for very small q could not be obtained by

TABLE I. Measured phonon frequencies for Mg_2Pb (THz).

Δ	Δ_5(TA)	Δ_1(LA)	Δ_5(TO)	$\Delta_{2'}$(LO)	$\Delta_{5'}$(TO)	Δ_1(LO)
0	0	0	5.10 ± 0.1	6.40 ± 0.08	6.40 ± 0.08	•••
0.1	•••	•••	•••	•••	•••	5.6 ± 0.1
0.2	•••	•••	5.12 ± 0.08	6.20 ± 0.15	6.28 ± 0.08	•••
0.4	1.14 ± 0.02	1.87 ± 0.05	4.81 ± 0.07	5.76 ± 0.20	6.25 ± 0.05	6.65 ± 0.15
0.6	1.44 ± 0.02	2.46 ± 0.07	4.60 ± 0.05	5.15 ± 0.10	6.26 ± 0.15	7.48 ± 0.10
0.8	1.50 ± 0.10	2.52 ± 0.07	4.4 ± 0.1	4.60 ± 0.05	6.40 ± 0.06	7.98 ± 0.08
1.0	1.51 ± 0.06	2.56 ± 0.05	4.24 ± 0.10	4.32 ± 0.08	6.50 ± 0.10	8.3 ± 0.3
Σ	Σ_3(A)	Σ_1(A)	Σ_3(O)	Σ_1(O)	Σ_3(O)	Σ_1(O)
0.05	•••	•••	•••	5.3 ± 0.1	•••	6.4 ± 0.1
0.1	•••	•••	•••	5.6 ± 0.1	•••	•••
0.2	0.98 ± 0.03	1.30 ± 0.04	4.96 ± 0.05	5.6 ± 0.2	6.3 ± 0.2	•••
0.4	1.61 ± 0.04	2.05 ± 0.08	4.64 ± 0.05	5.58 ± 0.15	5.79 ± 0.05	•••
0.6	2.00 ± 0.04	2.30 ± 0.10	4.30 ± 0.10	5.88 ± 0.10	5.30 ± 0.12	7.35 ± 0.30
0.8	2.40 ± 0.08	2.00 ± 0.08	4.30 ± 0.10	6.20 ± 0.12	4.64 ± 0.10	7.65 ± 0.15
0.9	2.55 ± 0.10	1.78 ± 0.08	•••	•••	•••	•••
Λ	Λ_3(TA)	Λ_1(LA)	Λ_3(TO)	Λ_1(LO)	Λ_3(TO)	Λ_1(LO)
0.05	•••	•••	•••	5.4 ± 0.1	•••	•••
0.08	•••	•••	•••	5.6 ± 0.1	•••	•••
0.1	0.48 ± 0.04	0.94 ± 0.08	5.08 ± 0.08	•••	•••	6.3 ± 0.1
0.15	0.78 ± 0.05	•••	•••	5.7 ± 0.1	•••	•••
0.2	0.95 ± 0.05	1.6 ± 0.1	5.12 ± 0.08	5.58 ± 0.12	6.06 ± 0.08	7.07 ± 0.10
0.3	1.15 ± 0.05	2.20 ± 0.08	5.40 ± 0.08	5.50 ± 0.15	6.00 ± 0.04	•••
0.4	1.22 ± 0.08	2.25 ± 0.08	5.37 ± 0.05	5.51 ± 0.06	5.75 ± 0.06	7.36 ± 0.15
0.5	1.19 ± 0.05	2.40 ± 0.08	5.56 ± 0.08	5.8 ± 0.1	5.72 ± 0.10	7.20 ± 0.10

the neutron scattering experiment. A frequency distribution function $g(\nu)$ was also computed from the model by the method developed by Gilat and Raubenheimer,[10] appropriately modified for the present model. The calculated histogram of $g(\nu)$ sorted into frequency channels of width $\Delta\nu = 0.02$ THz is shown in Fig. 2. Most of the critical points can be seen to correspond to the high-symmetry points. However, the sharp peak at 2.3 THz seems to be due to the region of the dispersion surface

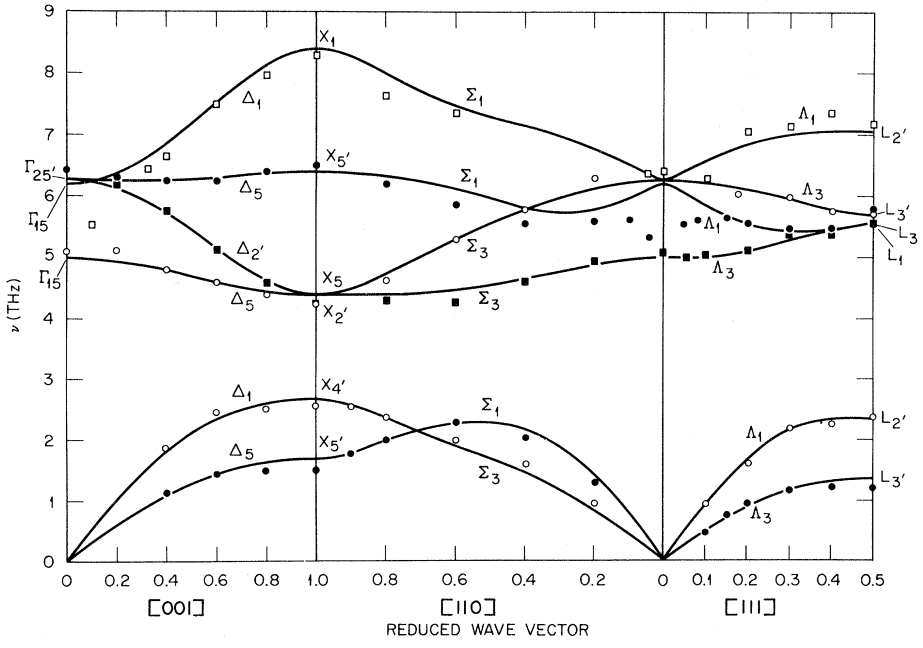

FIG. 1. Phonon-dispersion curves of Mg_2Pb for the principal symmetry directions. The solid lines are calculated dispersion curves from the nine-parameter shell model which was fitted to the experimental data.

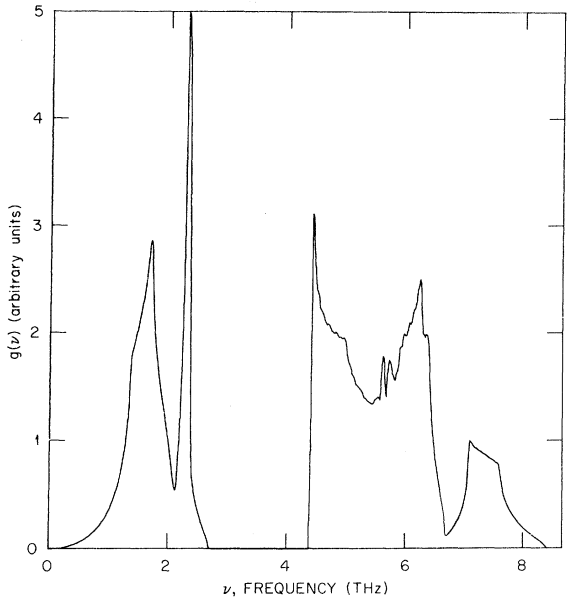

FIG. 2. Frequency-distribution function for Mg_2Pb calculated from the nine-parameter shell model.

near the maximum of the acoustic Σ_1 branch.

The Debye temperature Θ_D of Mg_2Pb has been measured by Schwartz *et al.*[11] as a function of temperature. The result shows that Θ_D decreases with temperature above 160 K, a trend also found for Mg_2Sn and attributed to anharmonic effects. Θ_D has been calculated using $g(\nu)$ obtained from the model and the result is shown in Fig. 3, together with the measured values. Also shown is Θ_D at 0 K estimated from the values of the elastic constants.[9] In the lower-temperature region, the calculated curve lies a few degrees below the measured points, probably because $g(\nu)$ was obtained from a room-temperature experiment.

TABLE II. Model parameters of shell model fit to the data. Short-range-force parameters are in units of e^2/V, where V is the volume of the unit cell and charge parameters are in units of e.

		Mg_2Pb	Mg_2Sn[a]
Mg-X	A_1	20.15	21.34
	B_1	−2.78	−3.00
Mg-Mg	A_2	0.066	0.24
	B_2	0.242	0.29
X-X	A_3	−0.303	0.10
	B_3	0.449	0.97
	Z_1	−1.993	−2.07
X	Y_1	−4.716	−4.90
	K_1	142.8	132

[a]Model II of Kearney *et al.* (Ref. 2).

V. CONCLUSION

Since over-all features of the dispersion curves for Mg_2Pb and Mg_2Sn are very similar, it is of some interest to calculate the phonon-dispersion curves using the parameters obtained for Mg_2Sn and the mass of Pb in place of Sn. It was found that the frequencies so calculated did not differ by more than 5% from those calculated using the parameters given in Table II for Mg_2Pb, except for the ΛTA branch for which the discrepancy is as large as 10%. In order to treat the lattice dynamics of Mg_2Pb more rigorously, it is necessary to use a theory of lattice dynamics of metals expressed

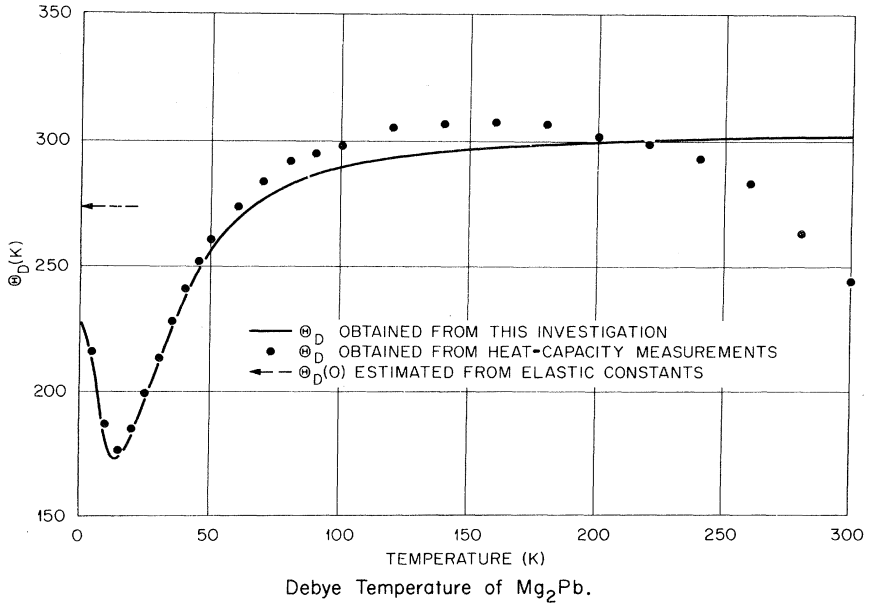

Debye Temperature of Mg_2Pb.

FIG. 3. Comparison of the experimental [Schwartz *et al.* (Ref. 11)] and calculated (nine-parameter shell model) temperature dependence of the Debye temperature of Mg_2Pb.

TABLE III. Elastic constants of Mg_2Pb calculated from the nine-parameter shell model (10^{11} dyn/cm^2).

	C_{11}	C_{12}	C_{44}
Model calc.	7.12	3.39	2.34
Expt.[a]	7.17	2.21	3.09

[a]Reference 9.

in terms of their electronic band structures. In its simplest form, the theory consists of a local effective potential and Hartree dielectric function of free electrons. However, it has been shown[1] that the Fermi surface of Mg_2Pb is quite anisotropic and, hence, it will be fruitless to discuss the lattice dynamics of Mg_2Pb using free-electron wave functions.

The almost cubic shape of the heavy-hole Fermi surface[1] may give rise to Kohn-type anomalies in the phonon-dispersion curves along the [001] direction. Although anomalies were not observed in the present experiment due to low intensities of scattered neutron groups, it would be interesting to carry out careful investigations of the dispersion curves of Mg_2Pb with various carrier concentrations. Also, similar experiments on Mg_2Si and Mg_2Ge would give us more information about the nature of the short-range interatomic forces in this family of compounds.

*Research sponsored by the U.S. Atomic Energy Commission under contract with Union Carbide Corporation and by the Ames Laboratory of the U.S. Atomic Energy Commission.

†Present address: PINSTECH, Rawalpindi, West Pakistan.

[1]G. A. Stringer and R. J. Higgins, Phys. Rev. B 3, 506 (1971).

[2]R. J. Kearney, T. G. Worlton, and R. E. Schmunk, J. Phys. Chem. Solids 31, 1085 (1970).

[3]R. J. Kearney, T. G. Worlton, and R. E. Schmunk, J. Phys. Chem. Solids 31, 913 (1970).

[4]J. M. Elridge, E. Miller, and K. L. Komarek, Trans. AIME 233, 1303 (1965).

[5]G. A. Stringer and R. J. Higgins, J. Appl. Phys. 41, 489 (1970).

[6]E. Anastassakis and C. H. Perry, Solid State Commun. 9, 407 (1971); Phys. Rev. B 4, 1251 (1971).

[7]E. Anastassakis and E. Burstein, in *Light Scattering in Solids*, edited by M. Balkanski (Flammarion, Paris, 1971).

[8]E. Anastassakis and C. H. Perry, in Ref. 7.

[9]P. L. Chung and G. C. Danielson, U.S. AEC Report No. IS-1451, 1966 (unpublished).

[10]G. Gilat and L. J. Raubenheimer, Phys. Rev. 144, 390 (1966).

[11]R. G. Schwartz, H. Shanks, and B. C. Gerstein, J. Solid State Chem. 3, 533 (1971).

PHYSICAL REVIEW B VOLUME 5, NUMBER 6 15 MARCH 1972

Electromechanical Effects in Metals

Paul Harris
Picatinny Arsenal, Dover, New Jersey
(Received 10 August 1971)

Existing first-order theory for the electrical voltage produced by shock loading a metal is extended to second order. The second-order result predicts a voltage where the first-order result does not. Experimental possibilities are mentioned.

INTRODUCTION

In 1965, Duvall and Thomson[1] (hereafter called DT) showed that first-order perturbation techniques predict no (i.e., zero) electrical signals resulting from mechanically shock loading a metal in an otherwise electrically inert solid. In other words, nothing similar to piezoelectric-type behavior is predicted.

Experimentally shock-induced electrical signals are seen in a great variety of materials (e.g., alkali-halides,[2] n-type Ge and Si,[3] and various plastics[4]), and the small-amplitude acoustic-type acoustoelectric experiments for single-frequency propagating waves have been explained theoretically.[5] The negative predictions of DT, in the light of the above-mentioned experimental and theoretical results, have bothered us now for some time. We have extended the work of DT to second order and find that a shock-induced electric voltage is predicted for a metal.

CALCULATION

DT expand the electron velocity at the top of the Fermi surface as

$$v = \sum_{n=0}^{\infty} B_n(x) P_n(\mu), \tag{1}$$

where μ is the angle of the electron velocity with respect to the direction of shock propagation, P_n